DOI: 10.1002/ejic.201601540

ChemPubSoc Europe

DOI: 10.1002/ejic.201601540

EurJIC European Journal of Inorganic Chemistry

Full Paper

Catalytic Hydrogen Peroxide Reduction

Improvement in Efficiency of the Electrocatalytic Reduction of Hydrogen Peroxide by Prussian Blue Produced from the $[Fe(CN)_5(mpz)]^{2-}$ Complex

Marcio C. Monteiro,[a] Kalil C. F. Toledo,[a] Bruno M. Pires,[a] René Wick,[b] and Juliano A. Bonacin*[a]

Abstract: Hydrogen peroxide is one of the most important molecules in chemical signaling in living organisms. Because of this, its sensing is indispensable for the diagnosis of many diseases. Among the materials used for the detection and quantification of H_2O_2, Prussian Blue (PB) has been highlighted due to its performance. Therefore, the search for alternatives or the improvement of PB performance is a challenge. In this context, our motivation was to evaluate how the ligand *N*-methylpyrazinium affects the structure and reactivity of Prussian Blue films produced from $[Fe(CN)_5(mpz)]^{2-}$ (PB-mpz). Based on the results, it was possible to conclude that the ligand is coordinated to the complex inside the PB framework and consequently contributes to the generation of a noncrystalline structure. The ions contained in buffer solutions can react with Prussian Blue by binding to Fe^{3+} and breaking the structure. In addition, a PB-mpz film in HCl/KCl showed higher sensitivity towards H_2O_2 than a PB film.

Introduction

The fast diagnosis of diseases can increase the chances of curing patients and contribute to minimizing the costs of treatments. In this sense, electronic devices such as point-of-care (POC)[1–3] allow fast and in situ diagnosis of patients without the need to transfer them to a hospital.[4,5] Besides the portability and simplicity of handling, the key point of POC devices is the design of specific responses to molecular targets.[6,7]

Among the most researched molecular targets, hydrogen peroxide deserves attention due its electrochemical response in oxidase biosensors and by the low level of detection.[8,9] H_2O_2 is a biomarker produced by (electro)chemical methods or by the oxidation of a target that is catalyzed by oxidases using O_2 as oxidizing agent,[10] as described in Figure 1.

Prussian Blue (PB) is widely used as a transducer in the sensing of H_2O_2.[9,11,12] In this approach, PB catalyzes the reduction of H_2O_2 and transfers the information to the electrode. As a result of these features, PB is known as an artificial peroxidase and it has been extensively studied in various fields of materials chemistry[13,14] and coordination chemistry.[15] Hence, the question emerges: Why study Prussian Blue?

Prussian Blue is one of the most ancient coordination compounds described in the literature and it still arouses fascination

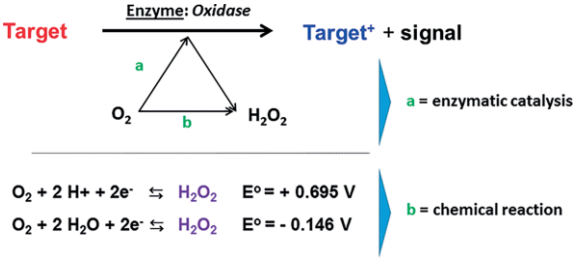

Figure 1. Production of hydrogen peroxide by the enzymatic catalysis of the oxidation of the analyte (target) and by the chemical/electrochemical method.

in scientists owing to its structure, which consists of Fe^{3+} coordinated to Fe^{2+} through a cyanide bridge in a cubic face-centered cell with space group *Fm3m*.[16] The electronic communication between metallic centers in different oxidation states produces an intervalence transition at around 680–730 nm; this causes the blue color and the electronic transition is assigned to t_{2g}^6-Fe^{II}, $t_{2g}^3e_g^2$-Fe^{III} → t_{2g}^5-Fe^{III}, $t_{2g}^4e_g^2$-Fe^{II}.[17]

The cavities formed in the PB structure and its analogues allow their use as hydrogen storage materials.[18] In addition, Prussian Blue is electrochemically active and can achieve different oxidation states (Fe^{2+}–CN–Fe^{2+} in Prussian White or Fe^{3+}–CN–Fe^{3+} in Berlin Green). Thus, it can be used in the cathodes of devices like fuel cells due to its capacity to promote the direct four-electron reduction of O_2 to H_2O,[19] known as the oxygen reduction reaction (ORR). Films of PB modify electrodes very well and are recognized through the formation of an electroactive layer. Owing to the electrochemical features of these films, PB is used in the detection and quantification of H_2O_2

[a] Institute of Chemistry, University of Campinas - UNICAMP, P. O. Box 6154, 13083-970, Campinas, SP, Brazil
E-mail: jbonacin@iqm.unicamp.br
www.lnanomol.iqm.unicamp.br
[b] Department of Chemistry, University of Zurich, Winterthurerstrasse 190, 8057 Zurich, Switzerland

Supporting information and ORCID(s) from the author(s) for this article are available on the WWW under http://dx.doi.org/10.1002/ejic.201601540.

and other analytes such as ascorbic acid,[15] cysteine,[20] and dopamine.[21] Consequently, PB can produce sensors used in the health care and food industries.

The challenge in the chemistry of Prussian Blue is to control its structure and reactivity and to identify the properties of this remarkable material. Considerable efforts have been made to control the structure, geometry, and size of PB crystals. Among them, we can describe some strategies for producing PB from pentacyanidoferrate(II) {PFC, $[Fe(CN)_5X]^{y-}$}.[15,22] Matsumoto et al.[23] reported that the incorporation of the ligand isonicotinamide into PB leads to materials displaying reversible electrochromic properties and selective channels in the structure. According to Ghasdian et al.,[24] it is possible to produce uniform nanocubes of PB at room temperature in the absence of surfactants or molecular templates by using pentacyanidoferrate(II).

The *N*-methylpyrazinium (mpz) ligand was chosen due to the strong interaction between the t_{2g} orbital of the metal and the π* antibonding orbital of the ligand in comparison with other N-heterocyclic ligands.[25] This feature leads to the formation of a very stable pentacyanidoferrate(II). Because of this, our motivation in this work was to evaluate the structure and reactivity of the *N*-methylpyrazinium-pentacyanidoferrate(II) $\{[Fe(CN)_5]^{2-}$ or PCF-mpz}, its ability to form Prussian Blue films, and the electrochemical behavior of the respective PB in the sensing of molecular targets.

Results and Discussion

Characterization of the *N*-Methylpyrazinium Iodide Ligand

Characterization of the mpz ligand is necessary to understand the behavior of PCF-mpz. The ligand mpz was characterized by ^{1}H NMR, electronic spectroscopy in the UV/Vis region, vibrational spectroscopy (FTIR), and electrochemical methods (see Section 1.1–1.4 in the Supporting Information). In cyclic voltammetry experiments, the mpz ligand undergoes irreversible reduction at low scan rates. On the other hand, at high scan rates (higher than 10 V s^{-1}), a process is observed that has been assigned to an electron transfer followed by a coupled chemical reaction (EC_i process), as proposed by Nicholson and Shain.[26] A complete description of the characterization and electrochemical behavior of the mpz ligand can be found in Sections 1.5 and 1.6 in the Supporting Information.

Electronic and Electrochemical Properties of the Complex PCF-mpz

The ^{1}H NMR spectrum of the complex (see Figure S9 in the Supporting Information) was recorded to compare with the spectrum of the ligand; the spectra show a shift of the signal of the protons assigned to the methyl group (H_a) from 4.53 to 4.08 ppm. Moreover, the signals assigned to the H_c and H_b protons of the pyrazinic ring shift from 9.01 to 8.17 ppm and from 9.45 to 9.71 ppm, respectively. The energies of the occupied and free orbitals of mpz are influenced by the coordination and the electron density around the H_c protons decreases, which result in a shift to lower field.[27]

The electronic spectra of the complexes PCF-mpz and PCF-amin $\{[Fe(CN)_5(NH_3)]^{3-}\}$ are presented in Figure 2A. The complex PCF-amin shows a weak band at 402 nm (ε = 4.26 × 10^2 L mol^{-1} cm^{-1}), which has been assigned to a ligand field transition (d–d).[15,28] When the amine is replaced by mpz a strong band appears at 661 nm (ε = 7.43 × 10^3 L mol^{-1} cm^{-1}), which has been assigned to a metal-to-ligand charge-transfer [MLCT; $Fe^{2+}(d\pi) \rightarrow mpz(p\pi^*)$] transition. The reported transition is responsible for the blue color of the complex.[25,29] A weak band at 382 nm also appears in the spectrum of the complex and can be assigned to a d–d transition (ligand-field transition).[30] The full electronic spectrum of the complex is shown in Figure 2B. All discussion on the characterization of PCF-mpz by vibrational spectroscopy can be found in the Supporting Information (Section 3).

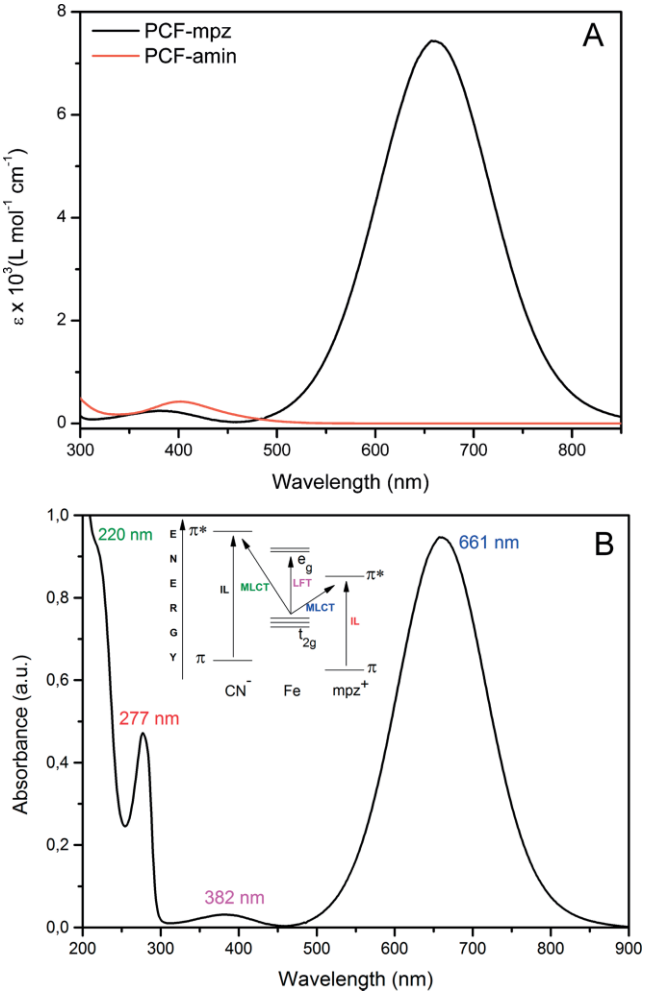

Figure 2. (A) Molar absorption coefficient as a function of the wavelength of PCF-amin and PCF-mpz. (B) Electronic spectrum (UV/Vis) of PCF-mpz in water.

Pentacyanidoferrates(II) show a well-defined electrochemical process that is influenced by the nature of the ligand. The obtained voltammograms for PCF-amin and PCF-mpz are shown in Figure 3A. The voltammograms reveal a redox process with $E^{o\prime}$ = 0.56 V versus Ag/AgCl, which has been assigned to the

$[Fe(CN)_5(mpz)]^{2-/3-}$ redox pair. All the potentials measured are consistent with the values reported in the literature.[15,25] The difference between the cathodic and anodic peaks indicates that the redox process is quasi-reversible (ΔE_p = 81 mV at a scan rate of 25 mV s^{-1}, see Table S4 in the Supporting Information).

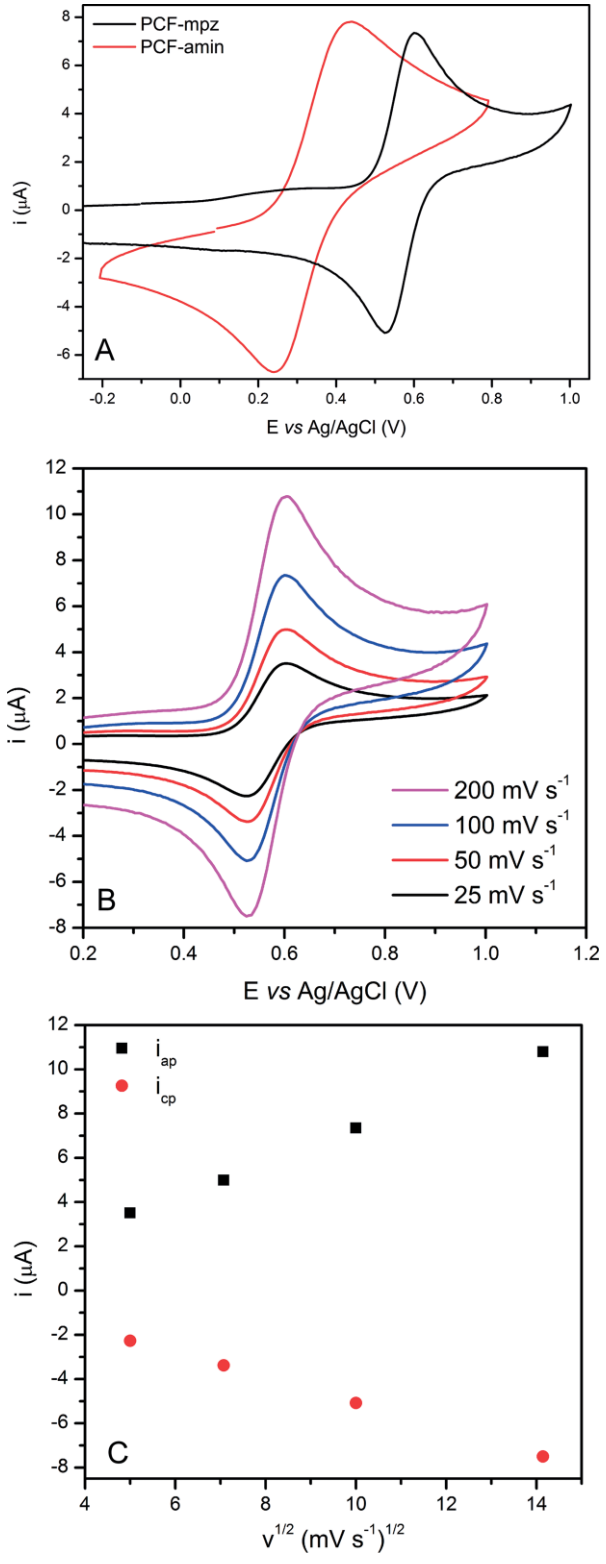

Figure 3. (A) Voltammograms of PCF-amin and PCF-mpz in water at a scan rate of 100 mV s^{-1} (supporting electrolyte 0.1 M KCl). (B) Voltammograms of an aqueous solution of PCF-mpz at different scan rates in 0.1 M KCl. (C) Relationship between current peak and scan rate.

The replacement of NH_3 by mpz in the complex changes the electronic density on the iron, as observed in the voltammograms in Figure 3A. The value of $E^{o\prime}$ for $Fe^{2+/3+}$ is shifted from 0.34 to 0.56 V versus Ag/AgCl and the increase in $E^{o\prime}$ reflects the greater acceptor character of the N-heterocyclic ligand as compared with NH_3.[31,32] Figure 3B shows the cyclic voltammograms of a solution of PCF-mpz in 0.1 mol L^{-1} KCl at different scan rates. The parameters obtained from the cyclic voltammetry experiments are listed and discussed in Table S4 and Section 4 in the Supporting Information. Figure 3C shows the relationship between current peak and scan rate. The peak current, and consequently $E_{1/2}$ and ΔE, do not change with increasing scan rate, which is a characteristic of a reversible process. However, the ratio between the cathodic and anodic current peaks (i_{ap}/i_{cp}) is far from unity at all scan rates. This can be explained by the lability of the oxidized form of PCF-mpz, which can slowly exchange the N-heterocyclic ligand for water without any apparent change in the potential measured,[31] but with a decrease in the cathodic current.

Another important point in reversible processes is the value of ΔE, which is expected to be between 60–65 mV, but ΔE = 81 mV was obtained for PCF-mpz. This increase in the separation of potential peaks represents a decrease in the heterogeneous electron-transfer rate (HET),[33] which can be assigned to the passivation of the electrode by non-electroactive materials, and thus the HET decreases. This evidences a problem in the control of the surface composition when a glassy carbon electrode is freshly polished, for example.[34] Finally, there is a regular variation in the current peaks with $v^{1/2}$ (Figure 3C), which indicates a mass-transfer process controlled by diffusion at slow scan rates.

Properties of the Prussian Blue Obtained from the Complex PCF-mpz

Electronic Spectroscopy

An electronic and vibrational spectroscopic study was performed to evaluate the differences and similarities between the Prussian Blue films prepared by traditional methods and those from complex PCF-mpz (FTIR spectra are discussed in Section 8 in the Supporting Information). The UV/Vis spectra of Prussian Blue (traditional) and Prussian Blue obtained from the complexes PB-mpz and PCF-mpz are compared in Figure 4. An intraligand transition from mpz is observed at 282 nm in PB-mpz, a redshift compared with that of PCF-mpz. LMCT transitions of PB are observed at 258 and 278 nm, and ligand field transitions are observed at 382, 400, and 401 nm for PCF-mpz, PB-mpz, and PB, respectively. An MLCT transition, $Fe^{2+}(d\pi) \rightarrow mpz(p\pi^*)$, is observed in the electronic spectrum of PCF-mpz and an intervalence transition (IT), Fe^{2+}–CN–Fe^{3+}, is found for PB. Moreover, PB-mpz presents both an MLCT at 573 nm (the coordination of Fe^{3+} to PCF-mpz causes the redshift observed) and IT at 708 nm.[23] A complete description of the wavelengths and transitions can be found in the Table S6.

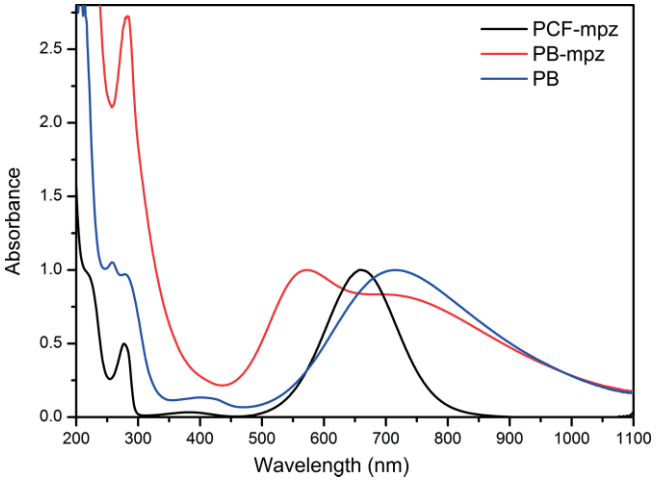

Figure 4. Comparison of the UV/Vis spectra of Prussian Blue (traditional), Prussian Blue obtained from the complexes PB-mpz and PCF-mpz. The absorbance values between 500 and 800 nm were normalized for the purpose of comparison.

Electrochemistry

Cyclic voltammetry was used to study the electrochemical behavior of glassy carbon electrodes modified with PB-mpz (Figure 5A). Thus, after immobilization of the compound, the potential was swept from –1.2 to 1.2 V versus Ag/AgCl in 0.1 mol L^{-1} KCl aqueous solution at a scan rate of 100 mV s^{-1}. PB was subjected to an identical process, with a smaller potential range (from 0.2 to 1.2 V) due to no redox processes being observed in the cathodic region of the voltammogram. The electrochemical parameters obtained are shown in Table S7 in the Supporting Information.

The reduction process of mpz (R1) can be seen at cathodic potentials. In this compound $mpz^{\cdot}$ looks unstable, similar to the voltammogram of free mpz (see Figure S4), but with an intermediate $E_{1/2}$ when compared with PCF-mpz and mpz ($E_{1/2}$ = –0.706 V vs. Ag/AgCl). This observation indicates that mpz is present in the structure. At cathodic potentials, PB and PB-mpz are in the reduced form [Prussian White (PW) and PW-mpz, respectively). Shifting to anodic potentials, PW and PW-mpz start to oxidize to PB and PB-mpz, respectively. CN^- is a good π-acceptor, but also a great σ-donor,[28] and consequently an increase in the charge density on Fe^{3+} facilitates the oxidation of this metal ($E_{1/2}$ = 0.196 V). For PB-mpz, due to the presence of mpz in the structure, some sites of Fe^{3+} are disabled to coordination with cyanide groups and these can be occupied by solvent (water). Because water has less σ-donor character than CN^-, Fe^{3+} has a smaller charge density than in PB. Thus, a small shift in the half potential is observed ($E_{1/2}$ = 0.219 V). Another important point is the width of the redox wave. It is much larger than that of PB, and includes a shoulder at 0.1 V. These factors indicate a different coordination by the Fe^{3+} and the shoulder can be assigned to a few Fe^{3+} atoms coordinated to six CN^-, as in traditional PB (i.e., there is a variation in the number of coordinated H_2O and cyanide). Also, these observations justify the increase in Δ*E*. The full-width at half-height (FWH) values for

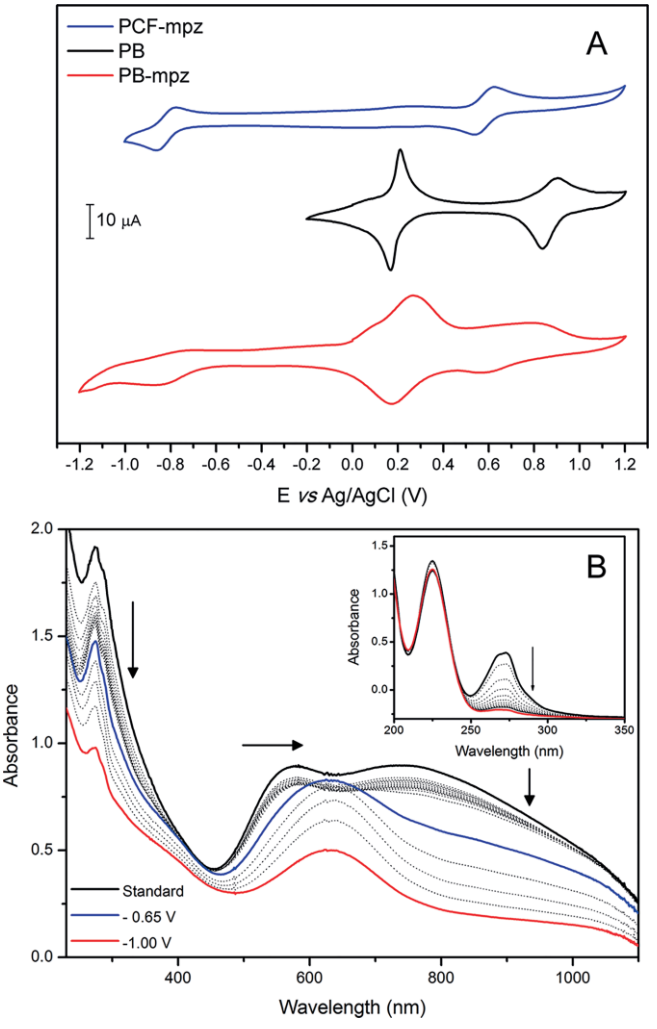

Figure 5. (A) Voltammograms of PCF-mpz (solution) and PB and PB-mpz films recorded at scan rates of 100 mV s^{-1} (supporting electrolyte 0.1 M KCl). (B) Spectroelectrochemistry of the PB-mpz film recorded sequentially at applied potentials of –0.65 and –1.00 V vs. Ag/AgCl. Inset: Part of the spectrum that corresponds to transition of mpz.

PB-mpz were found to be 226.6 and 216.5 mV for the anodic and cathodic processes, respectively (60.4 and 65.5 mV for PB). These values differ from the theoretical values (90.6/*n* mV) and may arise from lateral interactions, inhomogeneity of the surface sites, and ion interactions,[35] as well as evidencing the overlapping of multiple peaks.[23]

Increasing the potential during the sweep, some of the Fe^{2+} starts to oxidize and Berlin Green (BG, BG-mpz for the cyanidoferrate in this study) is formed. Thus, PB has an oxidation potential more positive than PB-mpz. This can be explained by the lack of cyanide bridges caused by the presence of mpz. In PB, the presence of Fe^{3+} decreases the charge density, increasing the bond length of Fe^{2+}–CN. This stabilizes the Fe^{2+}–C bond due to the lowering in energy of the t_{2g} orbitals, thereby increasing the oxidation potential (0.871 V). In the case of PB-mpz, the same is expected, but there is a lower number of cyanide bridges. Therefore, the CN bridge makes a higher contribution to the stabilization of the metal than the nonbridging

CN^- (and more than mpz, also). Consequently, the charge density on Fe^{2+} is higher in PB-mpz than in PB, increasing the energy of the d orbitals and decreasing the oxidation potential (0.677 V).

Spectroelectrochemistry

Based on the electrochemical behavior and considering the transitions assigned previously (see Table S6 in the Supporting Information), a spectroelectrochemical experiment was performed to confirm the assignments. The spectra are presented in Figure 5B. The first reduction of PB-mpz was performed at –0.65 V versus Ag/AgCl. The intervalence band disappears owing to the reduction of PB-mpz to PW-mpz (Fe^{2+}–CN–Fe^{2+}) and the MLCT band initially at 573 nm shifts to 625 nm. Upon the application of a voltage of –1.0 V, it is possible to observe a decrease in the intensity of the band at 625 nm. There is no process in the metallic centers and the reduction of mpz may contribute to the decrease in the intensity of the band assigned to MLCT.[23] Finally, the intensity of the band in the UV region decreases, which can be attributed to mpz transitions. To compare this transition, spectroelectrochemistry studies of mpz were performed (see inset in Figure 5B).

Determination of the Composition of PB and PB-mpz — Job's Method

An important aspect of this work was to identify the structure of PB-mpz and obtain some information on the ligand in the structure. A single crystal of this compound or computational calculations would support discussions. However, until now, only the structure of PCF-mpz has been solved.[36] On the other hand, a simple strategy to obtain information concerning the structure of PB-mpz involves the use of Job's method.[37,38]

Job's method was carried out by mixing aliquots of two equimolar solutions of metal and ligand. It was essential to keep the total analytical concentration of the reactants constant, varying only the ligand/metal ratio, as observed in Equation (1):

$$C_M + C_L = k \quad (1)$$

in which C_M and C_L are the analytical concentrations of the metal and ligand, respectively, and k is a constant. The corrected absorbance (Y) has been plotted as a function of the molar fraction of the ligand or metal. The resulting curve yields a maximum that indicates the ligand/metal ratio of the complex in solution. The corrected absorbance is defined by Equation (2):

$$Y = A - (\varepsilon_M C_M + \varepsilon_L C_L)b \quad (2)$$

in which A is the measured absorbance, ε_M and ε_L are the absorptivities of the metal and ligand, respectively, and b is the optical path length. Also, it is important to keep in mind that the molar fraction [Equation (3)] in this context is not the true molar fraction (the solvent is omitted from its calculation):

$$X_M = \frac{C_M}{C_L + C_M} \quad (3)$$

The molar fraction of the ligand is similarly defined.[37] In accord with the description above, Job's method was used to give some idea of the ratios of hexacyanidoferrate/Fe^{3+} (for PB) and PCF-mpz/Fe^{3+} (for PB-mpz). Thus, a region in the spectrum in which the intervalence band predominates was chosen. This way, it is possible to know the numbers of Fe^{3+} with cyanide bridges and, consequently, the stoichiometry of PB and PB-mpz. For PB, the absorbance was collected at 710 nm. Hexacyanidoferrate(II) (HCF) and ferric chloride do not exhibit any transition in the visible region of the spectrum and the value of the corrected absorbance is equal to the measured absorbance. For PB-mpz, owing to the intense MLCT band from PCF-mpz lying between the MLCT and IT wavelengths of PB-mpz (Figure 4), the chosen wavelength for this experiment was 850 nm, at which there is a small amount of MLCT overlap. Figure 6 shows the plot of Y versus $X_{Complex}$, in which $X_{Complex}$ represents HCF for PB and PCF-mpz for PB-mpz.

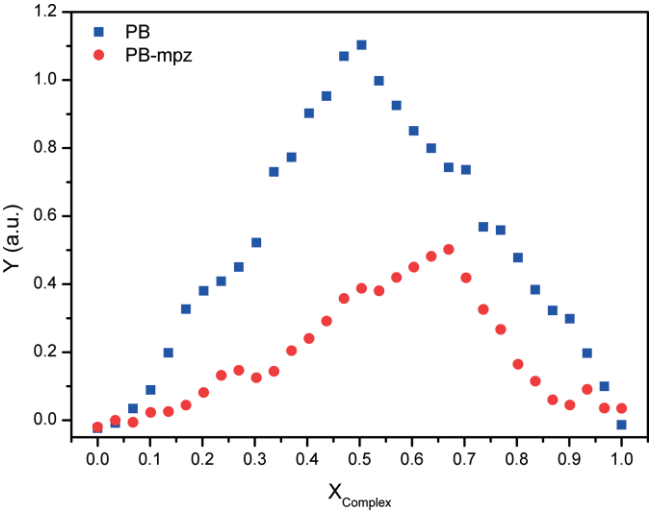

Figure 6. Job's plot obtained from the intervalence transition of ferric cyanidoferrate(II) (710 nm for PB and 850 nm for PB-mpz). $X_{Complex}$ = HCF for PB and PCF for PB-mpz.

Important information can be gained from this data. First, considering Beer's law, the maxima of the curves indicate a higher concentration of the product. Also, it is possible to observe some lower curves in both cases. This indicates that intermediate structures or byproducts are formed for different ratios of components. PB exhibits a broad maximum at X_{HCF} = 0.5, which indicates the formation of 1:1 HCF/Fe^{3+} under these experimental conditions. On the other hand, for PCF-mpz, a local maximum is observed at $X_{PCF\text{-}mpz}$ = 0.5 (Figure 6), and a maximum is observed at $X_{PCF-mpz}$ = 0.67 as the concentration of PCF-mpz is further increased; thus, a 2:1 PCF-mpz/Fe^{3+} ratio can be assigned. Secondly, the linearity of the segments in the Job's plots also indicates the formation of stable complexes. Based on these results, the chemical formula for PB and PB-mpz can be represented as $KFe[Fe(CN)_6]$ and $KFe[Fe(CN)_5(mpz)]_2$, respectively.

On the basis of these results, models of these complexes are presented in Figure 7. PB has a similar structure to that described in the literature,[39] with a 1:1 HCF/Fe^{3+} ratio. For comparison, part of the PB-mpz structure also was modulated in face-centered cubic unit cell (with a 2:1 PCF-mpz/Fe^{3+} ratio).

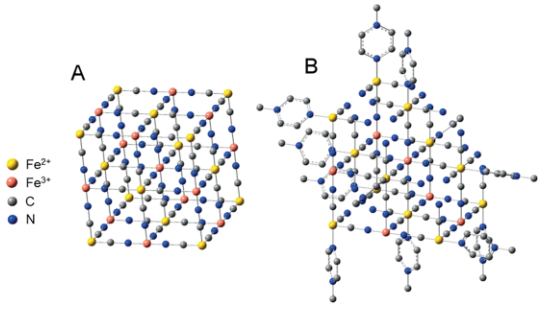

Figure 7. Proposed ferric cyanidoferrate(II) models: (A) PB with a 1:1 ratio and (B) PB-mpz with a 2:1 PCF-mpz ratio. Hydrogen atoms have been omitted for better views of the structures.

A significant number of defects in the structure can be seen (Figure 7B), but some factors need to be considered. One is the relative *trans* influence occasioned by mpz. CN^- *trans* to the ligand has a shorter length to Fe^{2+} due to the stronger σ-donation and π-receptor abilities of this group.[28,36] Then, when PB-mpz is formed, the stabilization of the d orbitals occasioned by the presence of Fe^{3+} weakens the Fe–mpz bond, facilitating ligand exchange. It was observed that the purple color of the PB-mpz solution turned blue after several hours. A discussion on the differences between the structures of PB and PB-mpz is found in the Supporting Information (Section 11).

Stability of PB-mpz Films in Buffer and Salt Solutions

The PB and PB-mpz films were prepared according to the method reported in the Supporting Information (Section 12). It was observed during the experiments that buffer solutions can decrease the stability of films of both PB and PB-mpz. Because of this, the PB films were tested in different buffer solutions, as summarized in Table 1. It was concluded that the salt ions of buffer solutions can react with Fe^{3+} ions. A complete discussion of the experimental results can be found in the Supporting Information (Section 13).

Table 1. Summary of the reactions of salt ions with PB films.

Salt ion	Fe^{3+}	PB	PB-mpz
Acetate	reacts[a]	reacts little	reacts
Borate	reacts[b]	reacts	reacts
Phosphate	reacts[b]	reacts	reacts
Sulfate	–	–	–

[a] Soluble product. [b] Insoluble product.

Electrochemical Stability of PB-mpz Films

Owing to the incompatibility of the anions discussed above, two buffer solutions were used to compare the stability of PB and PB-mpz films: HCl/KCl and Britton–Robinson (BR) buffer, both at pH 2.0. The stability of the films was established through several voltammetric cycles and evaluation of the current peaks of the redox processes of the immobilized species (Figure 8).

Both PB and PB-mpz-modified electrodes showed good stability after consecutive cycles, as presented in Table S8 in the

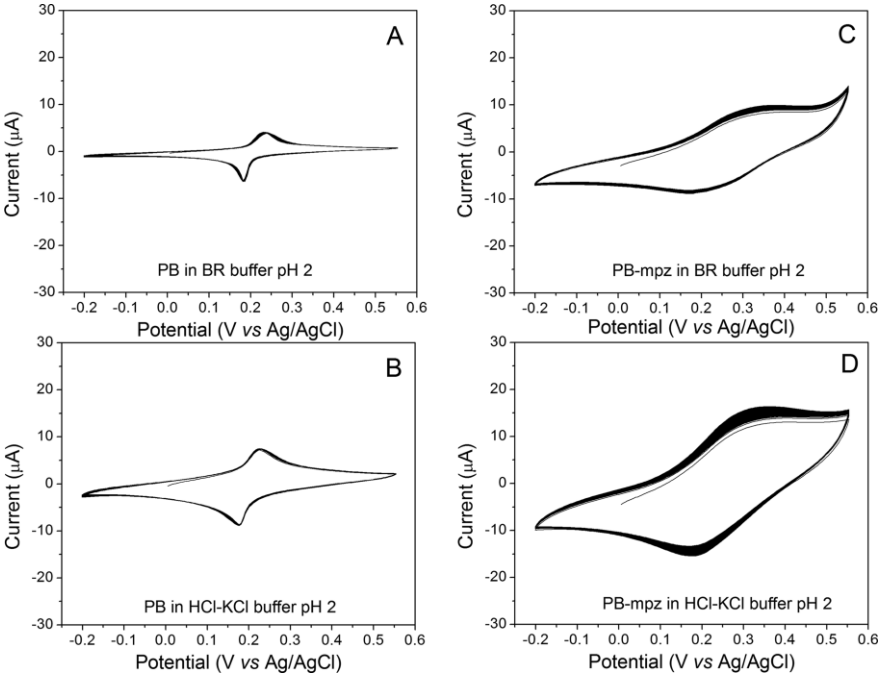

Figure 8. Stability of PB-modified electrodes in (A) BR and (B) HCl/KCl buffer solutions and of PB-mpz-modified electrodes in (C) BR and (D) HCl/KCl buffer solutions. Data collected in 0.1 M KCl as support electrolyte, scan rate = 50 mV s^{-1} and pH 2.0.

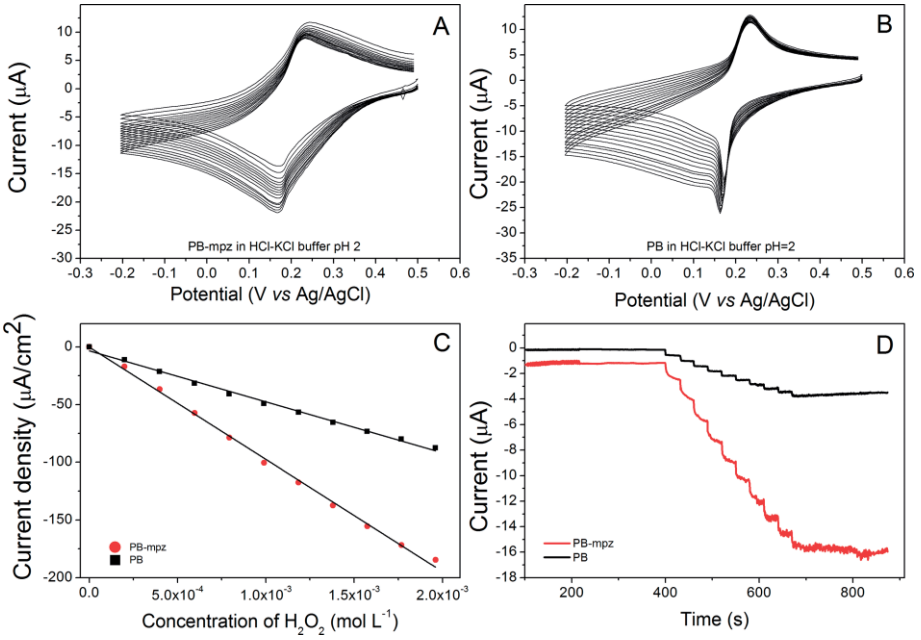

Figure 9. Electrochemical behaviour of electrodes modified by (A) PB and (B) PB-mpz in the presence of different concentrations of H_2O_2 in HCl/KCl buffer solution (pH 2.0). (C) Chronoamperometric detection of hydrogen peroxide using the modified electrodes in KCl/HCl buffer (pH 2.0), each addition corresponds to 20 μL of H_2O_2 (0.1 mol L^{-1}). Working potential: –0.1 and 0.18 V vs. Ag/AgCl for PB and PB-mpz, respectively. (D) Current density as a function of concentration of hydrogen peroxide determined by chronoamperometry.

Supporting Information. After the deposition step, the composition of the films is associated with the insoluble form of PB. However, multiple cycles of the redox system PB/PW lead to the soluble forms, due to the insertion of the potassium ion into the structure.[40] In addition, the H^+ ion can penetrate into the defects of the structures,[41] thereby decreasing the charge density around the iron ions and increasing the oxidation potential of Fe(N). On this basis, after the 100th cycle, it is possible to see that the oxidation potential of PB is increased by around 0.02 mV in BR buffer solution, whereas that of PB-mpz increases by around 0.11 and 0.05 mV in BR and HCl/KCl buffer, respectively. Consequently, the anions present in the BR buffer can affect the oxidation potential of PB-mpz. Moreover, the final current peak is lower than the initial value only for the PB film in BR buffer. Thus, owing to the high variation in the E_{ap} of PB-mpz and the small loss of the PB film in BR buffer, HCl/KCl buffer solution was chosen for the sensing studies of hydrogen peroxide.

Cyclic voltammetry experiments were performed to determine the best potential in chronoamperometric analysis (Figure 9A,B). Films of PB presented the best electrochemical response at –0.1 V versus Ag/AgCl. On the other hand, films of PB-mpz showed the best response at 0.18 V versus Ag/AgCl. These potentials correspond to the maximum current recorded in the electroreduction of H_2O_2 for each modified electrode.

The lowering of the potentials of PB films can be associated with the change in the composition of the films. The Fe^{2+} formed in the reduction process can rapidly react with H_2O_2 to produce Fe^{3+}, which may generate iron hydroxide if the pH of the solution is high or unbuffered, because the reduction of H_2O_2 can produce hydroxide ions. Another possible reason for decreasing PB film activity lies in the fact that PB can dissociate into HCF and $Fe(OH)_3$ under basic solutions or in unbuffered medium, but it is important to observe that both processes can be correlated.[42] Figure 9C shows the chronoamperograms of the modified electrodes after the addition of hydrogen peroxide and the corresponding analytical curves showing the variation of current density (Figure 9D) were obtained from the chronoamperograms.

The electroactive areas of the modified electrodes were determined (Equation S6 in the Supporting Information) before and after the cycles to compare their current density (Table S9). The results can be attributed to the greater surface area and defects in the PB-mpz structure in comparison with PB, in agreement with the results obtained by Job's method. An increase in the surface area or a change in the geometry of the PB films may also lead to a very low detection limit.[43,44] The PB-modified electrodes show a linear response to hydrogen peroxide reduction in the range of 0 to 2.5×10^{-3} mol L^{-1}. The limits of detection calculated for PB and PB-mpz were 1.11×10^{-4} and 7.39×10^{-5} mol L^{-1}, respectively. Therefore, PB-mpz shows several properties that differentiate it from traditional Prussian Blue.

Conclusions

According to the electrochemical experiments, the reduction of mpz produces the radical mpz$^{\cdot}$, which rapidly reacts with the medium, by an EC_i mechanism; the rate constant for the mpz$^{\cdot}$ reaction is 1.003×10^2 s^{-1}. In an acidic medium, the radical mpz$^{\cdot}$ reacts with H^+ to form a less reactive species in a quasi-reversible process. In addition, mpz coordinated to PCF renders the ligand less reactive, increases the oxidation potential of iron,

and produces a stable compound with a dissociation constant of 3.78×10^{-4} s^{-1}. Studies at of solutions at various pH have shown that PCF-mpz is more stable at pH < 7.0.

The formation of PB-mpz from PCF-mpz leads to a change in the electronic structures when compared with PB. Cyclic voltammetry has shown that the mpz ligand is present in the PB structure. Spectroelectrochemistry confirmed an IT band and a dislocation of the MLCT in reduction potentials. Job's method revealed ratios of 1:1 HCF/Fe^{3+} and 2:1 PCF-mpz/Fe^{3+}, which indicates the low crystallinity of the latter; XRD analysis confirmed that PB-mpz is an amorphous material. Experiments involving buffer solutions have shown that the PB-mpz structure can be broken depending on the nature of the ions present. Additionally, PB-based films were evaluated in BR and HCl/KCl buffers, with the latter producing a better electrochemical response. The PB-mpz film showed a higher sensitivity towards H_2O_2 than the PB film. The limits of detection were found to be 1.11×10^{-4} and 7.39×10^{-5} mol L^{-1} for PB and PB-mpz, respectively.

Experimental Section

Materials and Instrumentation

Pyrazine (99 %) and ammonium hydroxide (28 % m/v) were purchased from Sigma–Aldrich. Ethanol and sodium iodide were purchased from Merck. Sodium hydroxide (97 %), HCl (36.5–38 %), potassium chloride, and dimethyl sulfoxide were purchased from Synth. Sodium nitroprusside was purchased from Acros Organics. All other reagents and solvents were used as received, without further purification.

^{1}H NMR spectra of the ligand and PCF-mpz were recorded in deuteriated water with a Bruker Avance III 400 MHz (9.4 T) spectrometer. Electronic spectra were recorded with an HP Agilent 8453 spectrophotometer using a quartz cuvette with an optical path length of 1 cm. The measurements were performed at 25 °C in the range 200–1000 nm. The IR spectra of the iron complexes and mpz were recorded as KBr pellets with an MB 100 Bomem Spectrometer at a resolution of 2 cm^{-1} in the range 4000–400 cm^{-1}. Elemental analyses of the *N*-methylpyrazinium and pentacyanidoferrates were performed by using a CHNS/O Perkin–Elmer 2400 Analyzer.

Experimental Procedures

***N*-Methylpyrazinium Iodide (mpz-I):** Pyrazine ($C_4H_4N_2$, 2.0 g) was dissolved in methyl iodide (10 mL), the color changing to light red. The solution was kept at room temperature, without stirring and in the dark for 1 week, turning into a yellow solid. This solid was transferred to a rotary evaporator, heated to 60 °C, and ethanol (150 mL) was added until complete dissolution. The solution was filtered while hot and cooled to room temperature. The product was crystallized in an ice bath, forming large yellow needles that were filtered again with ice-cooled ethanol (15 mL). Yield: 75 %. $C_5H_7IN_2$ (222.03): calcd. C 27.05, H 3.18, N 12.62; found C 27.00, H 3.27, N 12.60.

$Na_3[Fe(CN)_5NH_3]\cdot 3H_2O$: Sodium nitroprusside {$Na_2[Fe(CN)_5NO]\cdot 2H_2O$, 6.0 g} was added to ammonium hydroxide (NH_4OH, 40 mL) in an Erlenmeyer flask (250 mL). The flask was stirred until complete solubilization of sodium nitroprusside. The flask was covered with aluminum foil and was stoppered with cotton to allow gas to exit. The solution was stirred in the dark for 3 h and the color turned dark yellow. For precipitation, sodium iodide (NaI, 6.0 g) was added and a yellow solid started to deposit on the bottom. Ethanol (100 mL) was slowly added to ensure complete precipitation. The solid was filtered, washed with ethanol, and dried on a vacuum line until constant weight. Yield: 74 %. $C_5H_9FeN_6Na_3O_3$ (325.98): calcd. C 18.42, H 2.78, N 25.78; found C 18.24, H 2.86, N 25.07.

$Na_2[Fe(CN)_5(mpz)]\cdot 4H_2O$: Amminepentacyanidoferrate (0.2 g) was dissolved in water (1 mL) and then mixed with a solution of the ligand (1 mL) in five-fold excess. The solution was cooled in an ice bath for 30 min in the absence of light and whilst stirring. The solution was treated with NaI (1.0 g) and, after complete dissolution, ethanol (30 mL) was added slowly, under intense stirring, until complete precipitation of the complex. The solid was filtered by using a vacuum pump, washed with ethanol, dissolved again in a solution of the ligand in two-fold excess, treated with further NaI (1.0 g), filtered, and stored in a desiccator. A constant weight was obtained after 1 week of drying. The complex is very hygroscopic. Yield: 86 %. $C_{10}H_{15}FeN_7Na_2O_4$ (399.10): calcd. C 30.09, H 3.79, N 24.57; found C 29.97, H 3.90, N 23.81.

Synthesis of the Ferric Cyanidoferrates: Ferric hexacyanidoferrate(II), known as Prussian Blue (PB), and ferric pentacyanidoferrate(II) (PB-mpz), prepared from the complex in this study, were synthesized by direct methods.[45]

Cyclic Voltammetry: Cyclic voltammograms were obtained with an Autolab EcoChemie PGSTAT20 potentiostat by using 0.1 mol L^{-1} potassium chloride (KCl) as supporting electrolyte in all measurements. A glassy carbon electrode was used as working electrode, an Ag/AgCl (in 3 mol L^{-1} KCl) electrode as reference electrode, and a platinum wire as auxiliary electrode. For each measurement, 5.0×10^{-3} mol L^{-1} solutions of the ligand and complexes were used. All the solutions were deaerated with nitrogen before the measurements. The potential range varied with compound and the scan rates used were 25, 50, 100, and 200 mV s^{-1}. Britton–Robson buffer solutions[46] were used for pH measurements.

X-ray Diffraction: X-ray powder diffraction analyses were performed with a Shimadzu XRD 7000 diffractometer with a copper tube operating at 40 kV and 30 mA. The divergence and scatter slits were of 1.0° and the receiving slit was of 0.30 mm. Scanning was performed in continuous mode, from 5 to 60° at a scan speed of 2° θ min^{-1}.

Influence of pH on the Stability of PCF-mpz: For studies of pH influence, solutions of the complex were prepared with concentrations of 1.0×10^{-4} mol L^{-1} in Britton–Robson buffer solutions. Electronic spectra were recorded every 30 s for 10 min at 25 °C. In this analysis, the spectrophotometer was equipped with an HP 89090A Peltier temperature controller.

Substitution Kinetics of mpz in the Presence of DMSO: Kinetics experiments of the substitution of mpz by dimethyl sulfoxide (DMSO) were performed by using the spectrophotometer equipped with a HP 89090A Peltier temperature controller. The absorbance of aqueous solutions of PCF-mpz in the presence of 0.5 mol L^{-1} DMSO (100 times in excess) was monitored. Spectra were recorded every 30 s for 1 h at 25 °C with controlled stirring. The ionic strength was adjusted with 1.0 mol L^{-1} NaCl,

Electrode Area Calculation: To calculate the electrode area, cyclic voltammetry analyses were performed. For each measurement, solutions of 1.0×10^{-2} mol L^{-1} hexacyanidoferrate(II) were used as a probe. All the solutions were deaerated with nitrogen before the measurements. The scan rates were 10, 25, 50, 100, and 200 mV s^{-1}. Equation S6 (Supporting Information, Section 4) was used to calculate the area.

Electrode Modification: Before modification, glassy carbon electrodes were polished by using an alumina slurry, rinsed with deionized water, washed ultrasonically, and cleaned again with deionized water. The electrodes were modified by the layer-by-layer drop-casting method. First, cyanidoferrate(II) solution (2.5 μL, 2.5×10^{-2} mol L^{-1}) was dropped on the electrode surface and dried for 30 min. Then ferric chloride solution (2.5 μL, 2.5×10^{-2} mol L^{-1}) was dropped on the cyanidoferrate(II)-modified electrode and this was dried again for 30 min. The second layer was the reverse: Ferric chloride solution (2.5 μL, 2.5×10^{-2} mol L^{-1}) was dropped on the PB-based electrode and dried for 30 min. Then cyanidoferrate(II) solution (2.5 μL, 2.5×10^{-2} mol L^{-1}) was dropped on the PB-based/Fe^{3+} electrode, which was then placed in a desiccator for 24 h. Thus, PB and PB-mpz were synthesized on the electrode surface from HCF and PCF-mpz, respectively. Before using, the electrode was washed with deionized water.

Spectroelectrochemistry: Spectroelectrochemistry data were obtained with a DropSens potentiostats and HP Agilent 8453 spectrophotometer. KCl (0.1 mol L^{-1}) was used as the supporting electrolyte. A platinum disc electrode was used as working electrode, a calomel saturated electrode as reference electrode, and a platinum wire as auxiliary electrode. The electrochemical cell has an optical path length of 1 mm.

Determination of the Stoichiometry of Prussian Blue: Job's analysis was performed by means of electronic spectroscopy. The absorbance of the mixture (acidic solution: 0.25 mmol L^{-1} of PCF-mpz and $FeCl_3$) was recorded varying the volumes of the reagents (from 0.0 to 3.0 mL). The final volume was kept constant (3.0 mL) to maintain the sum of concentrations constant.

Ferric Pentacyanidoferrates(II) in the Presence of Salt Solutions: PB and PM-mpz solutions were prepared with equimolar solutions of cyanidoferrate(II) and ferric chloride (5.0×10^{-3} mol L^{-1}). Sodium acetate ($NaC_2H_3O_2$), sodium borate ($Na_2B_4O_7$), sodium phosphate (NaH_2PO_4), sodium sulfate (Na_2SO_4), and ferric chloride solutions (0.1 mol L^{-1}) were prepared individually. For each compound (PB, PB-mpz, and $FeCl_3$), salt (acetate, phosphate, and sulfate) and deionized water were added, in salt/water ratios of 1:1, 1:2, and 1:3, respectively. Then the electronic spectra of each species were collected.

Stability of PB-Modified Electrodes: After modification, the electrodes were submitted to 25 cycles, removed from the solution for 10 min, and submitted to 100 more cycles. They were cycled in both Britton–Robinson and HCl/KCl buffer solutions (pH 2.0) separately. KCl (0.1 mol L^{-1}) was used as supporting electrolyte and the scan rate was 50 mV s^{-1} for both cycle experiments (potential range from –0.2 to 0.55 V).

Determination of Electrochemical Reduction Potential of H_2O_2: In an electrochemical cell, H_2O_2 (20 μL, 0.1 mol L^{-1}) was added to HCl/KCl buffer solution (pH 2.0). After 1 min, further H_2O_2 (20 μL, 0.1 mol L^{-1}) was added. This process was repeated several times to obtain a response curve. KCl (0.1 mol L^{-1}) was used as the supporting electrolyte and the scan rate used was 50 mV s^{-1} (potential range from –0.2 to 0.55 V vs. Ag/AgCl).

Chronoamperometry: Amperometric experiments were performed by using HCl/KCl buffer solution 10 mL) with 0.1 mol L^{-1} KCl as supporting electrolyte. The applied potentials were –0.1 and 0.18 V versus Ag/AgCl for PB and PB-mpz films, respectively. After current stabilization, H_2O_2 (20 μL, 0.1 mol L^{-1}) was added every minute to obtain the analysis curve.

Acknowledgments

The authors acknowledge the financial support of the Conselho Nacional de Desenvolvimento Científico e Tecnológico (CNPq) (grant no. 459923/2014-5), the Fundo de Apoio ao Ensino, à Pesquisa e à Extensão – Universidade Estadual de Campinas (FAEPEX-UNICAMP) (grant no. 2163/15), the Fundação de Amparo à Pesquisa do Estado de São Paulo (FAPESP) (grant no. 2013/22127-2), and CAPES.

Keywords: Electrochemistry · Reduction · Iron · Thin films

[1] P. Yager, G. J. Domingo, J. Gerdes, *Annual Rev. Biomed. Eng.* **2008**, *10*, 107.
[2] A. W. Martinez, S. T. Phillips, G. M. Whitesides, E. Carrilho, *Anal. Chem.* **2010**, *82*, 3.
[3] J. Hu, S. Wang, L. Wang, F. Li, B. Pingguan-Murphy, T. J. Lu, F. Xu, *Biosens. Bioelectron.* **2014**, *54*, 585.
[4] H. Shafiee, W. Asghar, F. Inci, M. Yuksekkaya, M. Jahangir, M. H. Zhang, N. G. Durmus, U. A. Gurkan, D. R. Kuritzkes, U. Demirci, *Scientific Rep.* **2015**, *5*, 8719.
[5] W. G. Lee, Y.-G. Kim, B. G. Chung, U. Demirci, A. Khademhosseini, *Adv. Drug Delivery Rev.* **2010**, *62*, 449.
[6] E. T. S. G. Silva, M. Santhiago, J. T. C. Barragan, L. T. Kubota, *Anal. Methods* **2014**, *6*, 6133.
[7] J. Wang, *Biosens. Bioelectron.* **2006**, *21*, 1887.
[8] A. A. Karyakin, O. V. Gitelmacher, E. E. Karyakina, *Anal. Lett.* **1994**, *27*, 2861.
[9] A. A. Karyakin, O. V. Gitelmacher, E. E. Karyakina, *Anal. Chem.* **1995**, *67*, 2419.
[10] A. A. Karyakin, *Electroanalysis* **2001**, *13*, 813.
[11] A. A. Karyakin, E. E. Karyakina, L. Gorton, *Electrochem. Commun.* **1999**, *1*, 78.
[12] Y. Lin, L. Hu, L. Yin, L. Guo, *Sensors Actuators B: Chem.* **2015**, *210*, 513.
[13] D. Kundu, E. Talaie, V. Duffort, L. F. Nazar, *Angew. Chem. Int. Ed.* **2015**, *54*, 3431; *Angew. Chem.* **2015**, *127*, 3495.
[14] M. Ishizaki, K. Kanaizuka, M. Abe, Y. Hoshi, M. Sakamoto, T. Kawamoto, H. Tanaka, M. Kurihara, *Green Chem.* **2012**, *14*, 1537.
[15] B. Morandi Pires, S. A. Venturinelli Jannuzzi, A. L. Barboza Formiga, J. Alves Bonacin, *Eur. J. Inorg. Chem.* **2014**, 5812.
[16] H. J. Buser, D. Schwarzenbach, W. Petter, A. Ludi, *Inorg. Chem.* **1977**, *16*, 2704.
[17] M. B. Robin, *Inorg. Chem.* **1962**, *1*, 337.
[18] M. P. Suh, H. J. Park, T. K. Prasad, D.-W. Lim, *Chem. Rev.* **2012**, *112*, 782.
[19] K. Itaya, N. Shoji, I. Uchida, *J. Am. Chem. Soc.* **1984**, *106*, 3423.
[20] L. Wang, S. Tricard, P. Yue, J. Zhao, J. Fang, W. Shen, *Biosens. Bioelectron.* **2016**, *77*, 1112.
[21] J. Li, Y. Jiang, Y. Zhai, H. Liu, L. Li, *Anal. Lett.* **2015**, *48*, 2786.
[22] J. T. Culp, J.-H. Park, D. Stratakis, M. W. Meisel, D. R. Talham, *J. Am. Chem. Soc.* **2002**, *124*, 10083.
[23] F. M. Matsumoto, M. L. A. Temperini, H. E. Toma, *Electrochim. Acta* **1994**, *39*, 385.
[24] N. Ghasdian, Y. Liu, R. McHale, J. He, Y. Miao, X. Wang, *J. Inorg. Organomet. Polym.* **2013**, *23*, 111.
[25] H. E. Toma, J. M. Malin, *Inorg. Chem.* **1973**, *12*, 1039.
[26] R. S. Nicholson, I. Shain, *Anal. Chem.* **1964**, *36*, 706.
[27] J. M. Malin, C. F. Schmidt, H. E. Toma, *Inorg. Chem.* **1975**, *14*, 2924.
[28] A. L. B. Formiga, S. Vancoillie, K. Pierloot, *Inorg. Chem.* **2013**, *52*, 10653.
[29] L. M. Baraldo, P. Forlano, A. R. Parise, L. D. Slep, J. A. Olabe, *Coord. Chem. Rev.* **2001**, *219–221*, 881.
[30] J. E. Figard, J. D. Petersen, *Inorg. Chem.* **1978**, *17*, 1059.
[31] H. E. Toma, C. Creutz, *Inorg. Chem.* **1977**, *16*, 545.
[32] K. J. Moore, L. Lee, G. A. Mabbott, J. D. Petersen, *Inorg. Chem.* **1983**, *22*, 1108.
[33] P. L. dos Santos, R. A. Timm, L. T. Kubota, J. A. Bonacin, *ChemistrySelect* **2016**, *1*, 1168.
[34] D. T. Fagan, I. F. Hu, T. Kuwana, *Anal. Chem.* **1985**, *57*, 2759.

[35] C. C. Corrêa, S. A. V. Jannuzzi, M. Santhiago, R. A. Timm, A. L. B. Formiga, L. T. Kubota, *Electrochim. Acta* **2013**, *113*, 332.
[36] B. J. Coe, S. P. Foxon, E. C. Harper, J. Raftery, R. Shaw, C. A. Swanson, I. Asselberghs, K. Clays, B. S. Brunschwig, A. G. Fitch, *Inorg. Chem.* **2009**, *48*, 1370.
[37] Z. D. Hill, P. Maccarthy, *J. Chem. Educ.* **1986**, *63*, 162.
[38] F. Woldbye, *Acta Chem. Scand.* **1955**, *9*, 299.
[39] H. J. Buser, A. Ludi, W. Petter, D. Schwarzenbach, *J. Chem. Soc., Chem. Commun.* **1972**, 1299.
[40] F. Ricci, G. Palleschi, *Biosens. Bioelectron.* **2005**, *21*, 389.
[41] V. Plichon, S. Besbes, *J. Electroanal. Chem. Interfacial Electrochem.* **1990**, *284*, 141.
[42] J.-M. Noël, J. Médard, C. Combellas, F. Kanoufi, *ChemElectroChem* **2016**, *3*, 1178.
[43] G. Liang, X. Li, S. Bao, H. Gao, F. Zhu, Q. Wu, *Polym. Chem.* **2015**, *6*, 4447.
[44] G. Liang, L. Zheng, S. Bao, H. Gao, F. Zhu, Q. Wu, *Carbon* **2015**, *93*, 719.
[45] L. Samain, F. Grandjean, G. J. Long, P. Martinetto, P. Bordet, D. Strivay, *J. Phys. Chem. C* **2013**, *117*, 9693.
[46] H. T. S. Britton, R. A. Robinson, *J. Chem. Soc. (Resumed)* **1931**, 1456.

Received: December 23, 2016